PIV on the flow of a simplified upper airway model

Mark Brouns[1], Sylvia Verbanck[2], Jeroen Van Beeck[3], Steve Vanlanduit[4], Joris Vanherzeele[5], and Chris Lacor[6]

[1] Department of Mechanics,Vrije Universiteit Brussel, Brussels, Belgium,E-Mail:mark.brouns@vub.ac.be
[2] Department of Pneumology,AZ-Vrije Universiteit Brussel ,Brussels, Belgium,E-mail:Sylvia.verbanck@az.vub.ac.be
[3] Von Karman Institute for Fluid Dynamics, Sint-Genesius-Rode, Belgium, E-mail:vanbeeck@vki.ac.be
[4] Department of Mechanics,Vrije Universiteit Brussel, Brussels, Belgium, E-mail:svanlandui@vub.ac.be
[5] Department of Mechanics,Vrije Universiteit Brussel, Brussels, Belgium, E-mail:jvherzee@vub.ac.be
[6] Department of Mechanics,Vrije Universiteit Brussel, Brussels, Belgium, E-mail:chris.lacor@vub.ac.be

Abstract Inhaled medication is available since many years for the treatment of asthma and other chronic pulmonary diseases. It is important that the aerosols containing the medications effectively reach the alveolar zone of the lungs. A certain part of the dose will deposit on the walls of the extra-thoracic airways (mouth-throat zone). This passage has a highly irregular shape with a mouth section, a 90 degree bend and the passage through the vocal cords. When the air enters the mouth by inhalation it passes through the pharynx and enters the trachea via the larynx which contains the epiglottis and the vocal cords. The severe constriction caused by the vocal cords causes the flow to accelerate resulting in a laryngeal jet. From CT-scans, taken at every 0.5 mm of several human subjects during the inspiration phase of the inhalation cycle, an "idealized" geometry of the human upper airways was created. From this non-scaled geometry a "negative" kernel was generated by use of stereo-lithography. Then, a non-transparent silicone mould was fabricated wherein a low-melting point alloy was poured. The corresponding "positive" is obtained by casting the kernel in a transparent silicone block.

The use of PIV to measure an internal flow requires non-reflecting boundaries since reflections cause distorted images near the boundaries. Therefore, the refraction indices of the fluid and the silicone should match. When using a glycerin-water solution for the fluid this property is satisfied. To obtain the same Reynolds number as in the real air flow conditions, the velocity will be scaled down because kinematic viscosity of the solution is approximately 3 times lower.

The velocity field is measured in a transversal plane at three different flow rates, 40 l/min, 20l/min and 13.3 l/min air flow rate. These flow rates represent normal breathing and quiet breathing

1. Introduction

Inhaled medication is available since many years for the treatment of asthma and other chronic pulmonary diseases. The advantage of pulmonary drug delivery through inhalation has recently led to the development of a series of new aerosol medication. For some medications, this kind of drug administration is chosen because it offers topical treatment of a specific lung condition while limiting whole-body effects.

It is important that the aerosols containing the medications effectively reach the alveolar zone of the lungs. A certain part of the dose will deposit on the walls of the extra-thoracic airways (mouth-throat zone).

By inhalation air enters the mouth, passes through the pharynx and flows into the trachea via the glottal region. The flow in these regions is highly irregular owing to the complexity of the airway structure.

The complexity of extra-thoracic airway flow field makes the study of the flow in the airways a challenge for both experiments [6] and Computational Fluid Dynamics (CFD).

Several experimental studies have been performed. Gemci et al. [3] compare experimental and

numerical characterizations of the turbulence levels within a simple throat model. They demonstrated that the asymmetrical laryngeal jet and the subsequent recirculation regions influence the spray dynamics and spray deposition patterns within the larynx and trachea. Corcoran et al. [2] studied the laryngeal jet from the cadaver of an adult female and noted the importance of downstream conditions on the position of the laryngeal jet. Endoscopic paricle image velocimetry (PIV) measurements on a simplified model of the throat were perfomed by Heenan et al. [6]. The velocity field in the central sagittal plane was studied during steady inspiration. Those measurements were compared with CFD predictions to note that the results were in poor agreement owing to deficiencies in CFD modeling.

Numerous attempts are made to characterize the flow in the airways by use of CFD, mainly using Reynolds-averaged Navier-Stokes (RANS) modeling methods. Yu *et al.* [14] and Martonen et al. [11] studied the airflow patterns in the upper airways which included nasal, oral, laryngeal and the first two generations of the tracheobronchial airway. Effects of breathing patters, i.e., nasal breath, oral breath and simultaneously nasal and oral breath, on the airflow of ultra fine particles were investigated. It was seen that although breath patterns have great impact on velocity distributions in laryngeal airways, the velocity profiles within the trachea and tracheobronchial airways were very similar and virtually independent of the breath patterns. Renotte et al. [13], Katz et al [7] and Brouns et al [1] concentrated on the analysis of larynx/trachea region as it has a major influence on the fluid and deposition dynamics of the whole respiratory system. It was noted that the larynx has pronounced effects on the motion of air in the trachea. Also, the flow inside the larynx is very complex including eddies in the lumen and reverse motion along the surface. These features tend to increase the residence times of entrained drug particles.

Zhang et al [15] verified their numerical simulation data with experiments where the fraction of the deposition is measured. Matida et al [10] state that the Eddy Interaction Model (EIM) (Gosmann and Ioannides [4]) had to be modified in order to obtain improved agreement with the experiment. While Zhang et al [15] claim that the EIM is adequate but the turbulence model doesn't satisfy. Therefore, it is important to first fully understand the fluid flow in the human upper airways and to characterize the turbulence levels in the pharynx, larynx and the trachea.

2. Model preparation

Data provided by the Department of Pneumology of the academic hospital of the Vrije Universiteit Brussel., of several male subjects during the inspiration phase of the inhalation cycle, were imported into the Amira software and smooth 3D-geometries were created. These data contained cross-sectional CT-scans of the upper airways at every 5 mm. Specialists in the field of human respiration selected the most appropriate realistic geometry. Figure 1 shows such a view of a CT-scan. By use of Computational Fluid Dynamics (CFD) simulations, an idealized 3D geometry was created in such a way that the main flow characteristics were preserved (Figure 2).
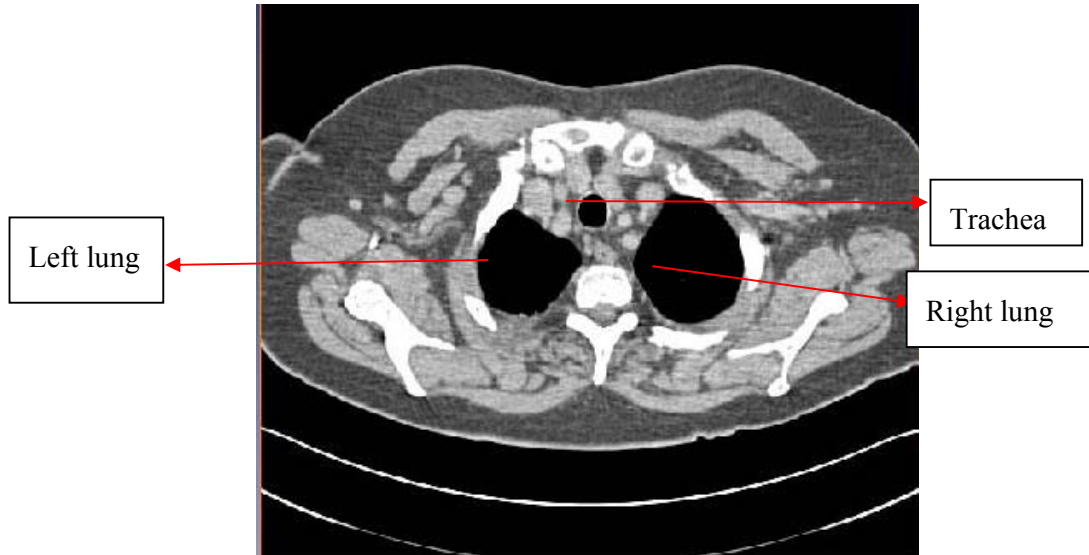
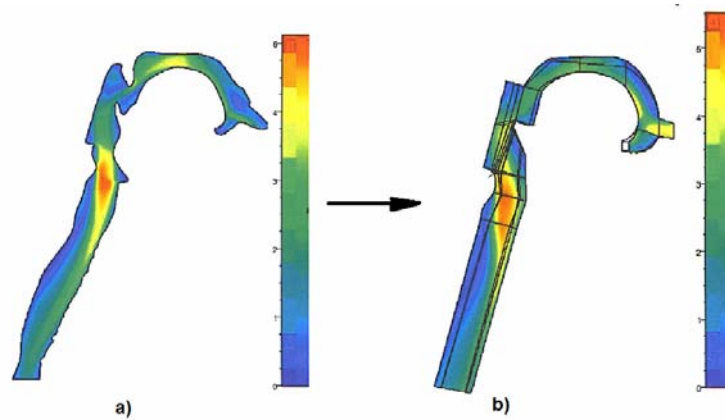**Figure 1: example of a CT-scan**

Figure 2: magnitude of velocity in a central sagittal plane, simulations performed with CFD

From this non-scaled idealized geometry a "male" kernel was generated by Materialise using stereo-lithography. Then, a 2-block non-transparent silicone mould was fabricated wherein a low-melting point alloy MCP 70 (Mining & Chemical product, Wellingbourough) was poured (Figure 3a). The corresponding male metal model is tooled to get a smooth surface (Figure 3b). This male model is then placed in a Perspex box.

A liquid mixture of silicone (base + curing agent) (Silicone Elastomer Sylgard 184, Dow Corning, USA) is poured into the box, surrounding the male model. The liquid silicone was very viscous and as a result contained many air bubbles after mixing base and curing agent (Figure 3c).
For that reason the silicone had to be de-aired before it was let to dry. Finally, the metal was removed with hot water and a female model of the idealized human upper airways was obtained.
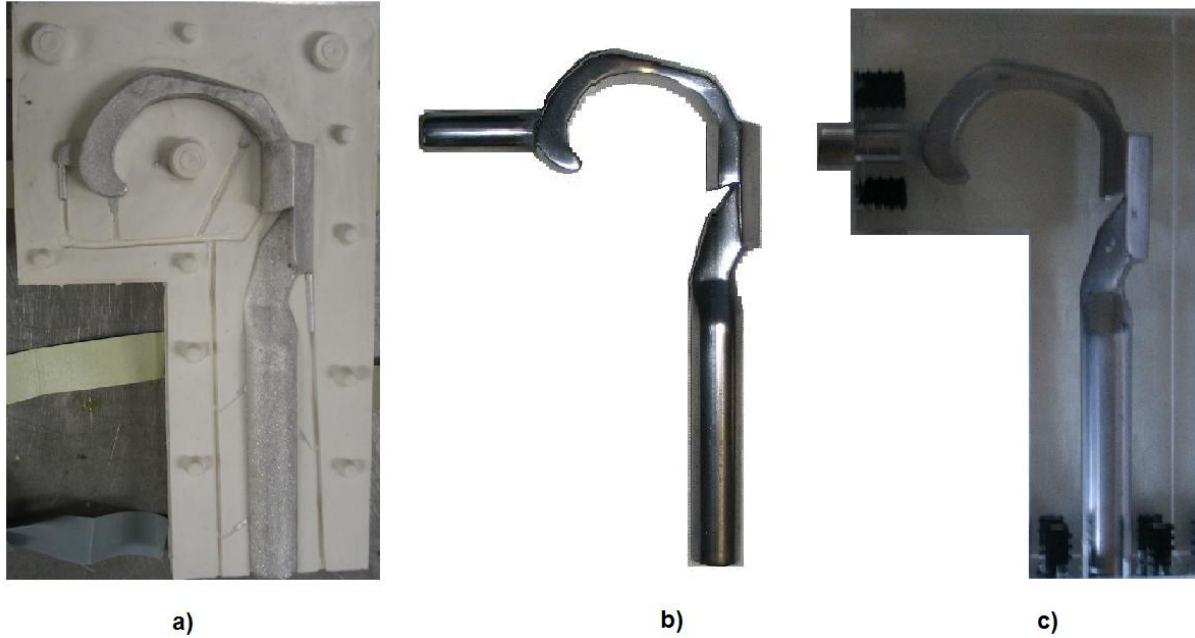
Figure 3: a: Male metal model in Silicone mould; b: Tooled metal model; c: Metal model inside transparent silicone block

3. Experimental Set-up

The use of PIV to measure an internal flow requires non-reflecting boundaries since reflections cause distorted images near the boundaries. Therefore, the refraction indices of the fluid and the silicone should match. Subsequently a mixture of water and glycerin was used to match the refraction index. The refractive index of the cured silicone differs from model to model and it is necessary to check the matching of the refractive index for both model and fluid empirically. Hence, a sheet with gridlines was placed behind the model and mixture with excess glycerin was pumped throughout the system. When looking through the model and the mixture, the gridlines are deformed. By adding water to the mixture, the distortion slowly decreases until it totally disappears. This is the point where mixture and model have the same refractive index.

The viscosity of the glycerin/water mixture had to be known, so that Reynolds number matching could be applied. The viscosity of the mixture depends on temperature and had to be accurately measured at operating temperature, which was around 27.3°C. The viscosity of the mixture was $5.38 \ 10^{-6} \ m^2$ /s measured with the AVS300 viscosimeter from Schott Geräte at 27.3°C. The model is not scaled and consequently the Reynolds number matching amounts to:

$$Q_{air} = \frac{v_{air}}{v_{mixture}} Q_{mixture} \tag{1}$$

where Q is the volumetric flow rate and v is the kinematic viscosity.

Measurements were performed in a central sagittal at three different flow rates: 40, 20 and 13.3 l/min air flow rate representing quit breathing (13.3 l/min) and normal breathing (20 to 40 l/min). Figure 4 gives schematic diagram of the experimental set-up.
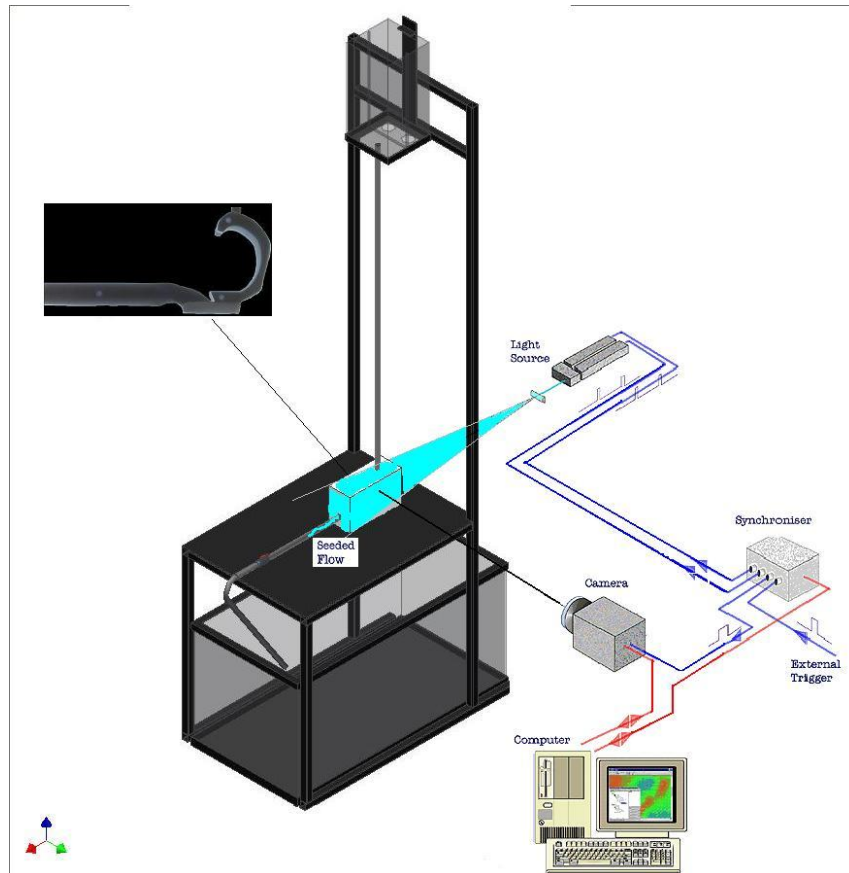
Figure 4: Experimental set-up

The fluid was pumped in a reservoir placed approximately 1.5 meter above the model in order to create a developed velocity profile. The outlet of the reservoir is separated from the inlet, which is connected to the pump and the overflow pipe, which guarantees a constant level in the reservoir, by a fine maze to stabilize the level and to remove the fluctuations caused by the pump.

4. Method

At the outlet of the model a tube with an orifice meter was connected. To regulate the flow rate a valve was set at the very end, behind the orifice meter.

New Wave MinilaseII Nd-Yag laser (532 nm wavelength, 100mJ/pulse) was synchronized with a pulse separation, depending on the flow rate. The pulse separation was chosen in such a way that the reflection of the tracer particles (10 μm hollow glass spheres) shift 3 pixels between an image pair. The laser beams were combined and formed into a sheet with cylindrical optics. This "pulsed" sheet was passed through the model, parallel to the flow, and the light scattered from the particles was recorded with a PCO sensicam QE 5Hz camera.

Approximately 30 series of 140 images each, resulting in 4000 image pairs were recorded. The interframing time was determined in such a way that an nearly optimal particle displacement (approximately 3 pixel displacement between two consecutive images) in the higher flow regions was obtained. The images were analyzed using PIVview 1.7 software package from PIVTEC GmbH, Göttingen Germany. The vector fields were generated using cross-correlation fast Fourier

transform (FFT) with an adaptive multi-pass procedure. A double correlation ('Hart correlation'), first proposed by Prof Doug Hart was applied to increase detectability of the correlation peak associated with the particle shift[5].

The interrogation region was 32x32 pixels on each pass with an overlap of 50%. After the first pass, the vector field was filtered for outliers using a maximum pixel displacement difference of 3 pixels. Only 0.1% of the vectors (typically 1 vector in the field) had to be interpolated. A least squares 3-point Gauss fit algorithm was used to recover the sub-pixel displacement of the correlation. Since it uses more data for the location of the peak the noise in the result is generally less compared more simple fits.

A combination of image parameters and numerical effects influence the uncertainty and systematic error in the displacement estimation for a given interrogation region using a cross-correlation FFT. The magnitudes of the displacement correlation peak moves from the center to the correlation region [8]. The multi-pass algorithm reduces the uncertainty and the measurement noise significantly when the particle image displacement is less than half a pixel (RAFFEL et al.).

The typical interrogation region parameters were:

- average particle image diameter: 2 to 4 pixels
- an average pixel displacement: 3
- Number of particles: 6-8

According to Raffel et al. [12] this results in a RMS random error less than 0.05 pixels (2 % of the average displacement). There are no systematic errors expected.

Figure 5 shows a histogram of pixel displacement in a randomly chosen image pair. Inspection of the histogram showed no evidence of peak-locking
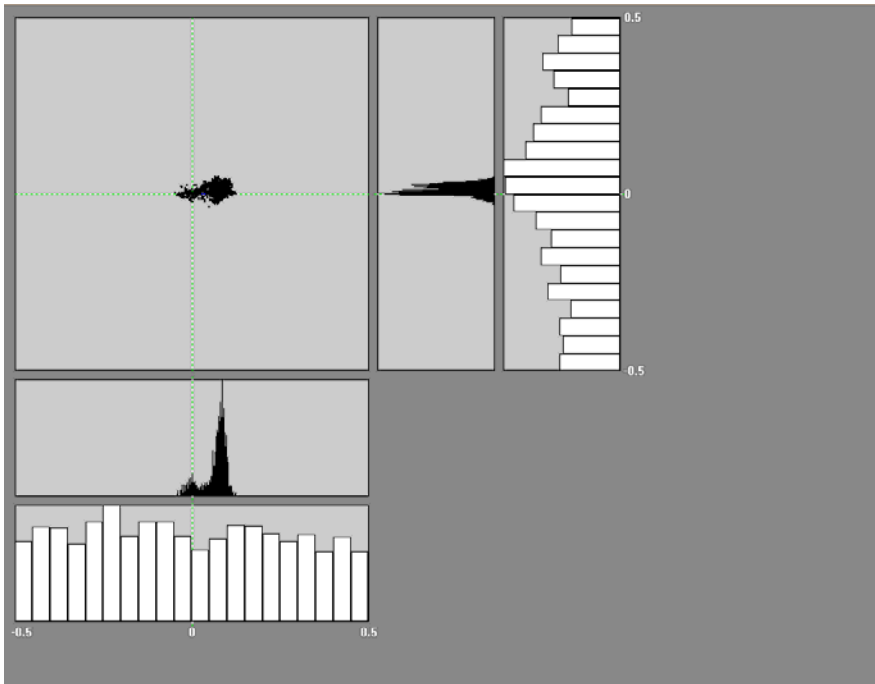

Figure 5: histogram of pixel displacement data in x and y direction of a randomly chosen image pair

The quality of the measurements done at an air flow rate of 13.3 l/min is not as good as at the other two flow rates. The flow rate was so low that particles got stuck at the walls and gave lot of reflection problems. Therefore only a section at the end of the larynx and beginning of the trachea was measured.

5. Results

The results of the measured magnitude of velocity and the streaklines for 20 l/min and 40 l/min are presented in figure 6. The flow is characterized by three major zones of recirculation, in the mouth, the pharynx and the trachea. The two recirculation regions in the mouth are caused by the sudden change in flow direction from the inlet tube to the mouth. The flow impinges on the tip of the tongue and follows the tongue to the end where it turns into the pharynx. Heenan et al also report the formation of a separation bubble at the roof of the mouth but it is a lot smaller. This is probably due the major difference in geometry, compared to the present model of the mouth. The beginning of the pharynx resembles a backward facing step. This explains the formation of a recirculation at the upper end of the pharynx. The epiglottis valve guides the flow towards the back of the pharynx. For that reason a separation bubble forms at the top of the epiglottis valve. The change in cross-sectional area causes the flow to accelerate. This acceleration increases even more when it reaches the glottic region and results in a jet. This so-called laryngeal jet impinges on the anterior side of the trachea and follows this wall to the end of the trachea. At the anterior side of the trachea a huge separation bubble is formed. The formation of this laryngeal jet is described by several authors. Corcoran and Chigier and Renotte et al found the jet to be at the posterior side of the trachea. Katz and Martonen and Kleinstreuer and Zhang describe the formation of this jet in the center of the trachea. Heenan et al claim that the jet is formed at the anterior side of the trachea. In Brouns et al it was found that the location of the jet depends on the geometry of the glottis and the overall mouth-throat geometry.

The streaklines in figure 6, show a possible existence of three dimensional flow. In fact, when visualizing the flow with air bubbles the flow is bent first under the tongue and turns upwards to roof of the tongue.
Figure 7 gives a view of the normalized turbulent kinetic energy in a central sagittal plane at two different flow rates. On the left panel of the figure, the results of the 20 l/min air flow rate are shown while on the right panel the results of the 40 l/min air flow rate are visualized.
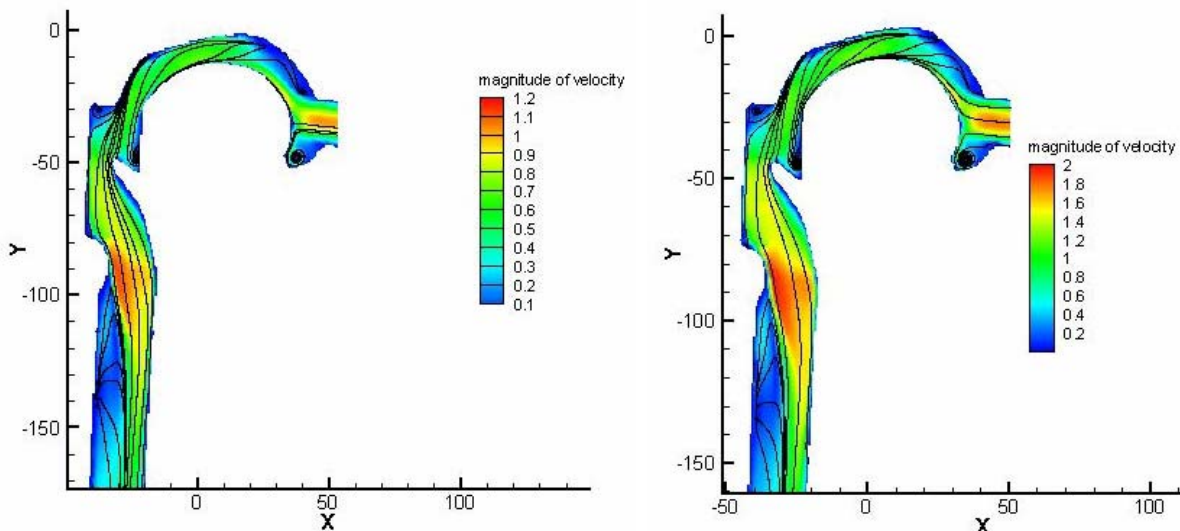

Figure 6: Magnitude of velocity and streamlines in an idealized model of the upper human airways (left: 20 l/min air flow rate; right: 40 l/min air flow rate)

The turbulent kinetic energy is defined by:

$$k_{norm} = 0.5 \frac{u_{rms}^2 + v_{rms}^2}{U_{inlet}^2} \tag{2}$$

where k_{norm} is the normalized turbulent kinetic energy , u_{rms} and v_{rms} are the fluctuating components of velocity. Because the measurements are done in two dimensions, the third fluctuating component w_{rms} is missing. As a result the turbulent kinetic energy is underestimated. However some interesting conclusions can be drawn.

At the inlet the turbulence level is very low in both flow rates. The Reynolds number based on the inlet ranges from approximately 1700 for the 20 l/min air flow rate and approximately 3000 for the 40 l/min air flow rate, at the inlet. And therefore low values of the normalized turbulent kinetic energy are to be expected.

In the oral cavity the turbulent kinetic energy are relatively low. When going downstream the level of kinetic energy rises and is higher in the shear layers in the pharynx. The tracheal jet and the recirculation which is linked with it, form a shear layer, where the turbulence levels are the highest throughout the model.
Comparing the results of both flow rates, the difference in turbulence levels and shape of the velocity magnitude are not really noticeable.
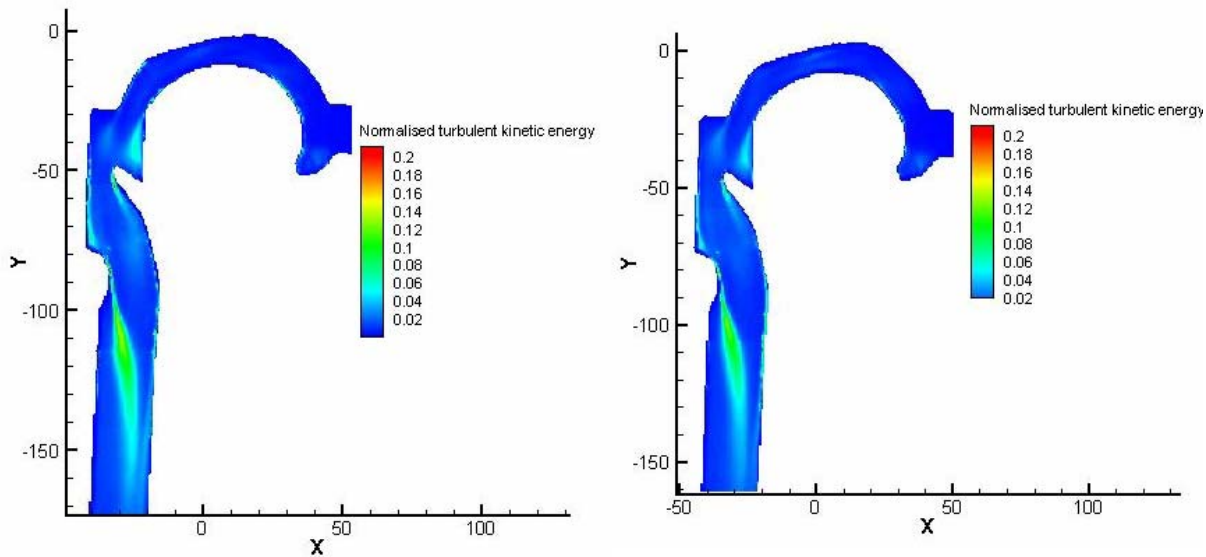

Figure 7: Normalized turbulent kinetic energy in an idealized model of the upper human airways (left: 20 l/min air flow rate; right: 40 l/min air flow rate)

The left panel of figure 8 shows a view of the magnitude of velocity in a central sagittal plane on the larynx at a flow rate of 13.3 l/min. The laryngeal jet expands more slowly at this low flow rate compared to the other two flow rates. This is also observed in the phase Doppler study of the laryngeal jet of Corcoran et al.
There is still a zone of considerably high normalized kinetic energy, as shown on the left hand side of figure 8, nevertheless the flow is laminar at inlet of the model.
The zone of high normalized turbulent kinetic energy in the shear layer of the laryngeal jet is narrower and is shifted more to the end of the trachea compared to the region of higher turbulent kinetic energy in the other two flow rates.
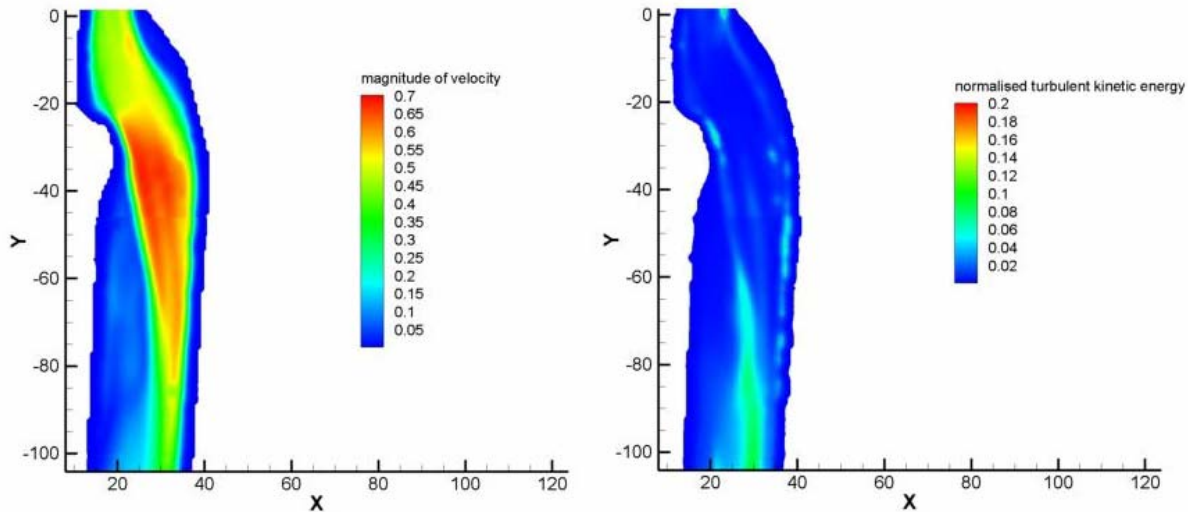
Figure 8: Magnitude of velocity (left) and normalised turbulent kinetic energy (rigth) in a central sagittal plane of the larynx at 13.3 l/min air flow rate

5. Conclusions

An idealized model of the upper human airways was successfully developed and an experimental model was created. Via Reynolds similitude, three different inhalation flow rates (13.3, 20 and 40 l/min) were measured in a central sagittal plane by the use of PIV.

The results show the complex nature of the flow in this idealized model. Several regions of recirculation in mouth, pharynx and trachea show the possible existence of three dimensional flows.

The normalized turbulent kinetic energy in the central plane at an air flow rate of 40 and 20 l/min is very similar while in the case of 13.3 l/min the region is shifted towards the end.

The laryngeal jet in case of 20 and 40 l/min air flow rate decays faster and is a little bit wider compared to the jet in case of 13.3 l/min air flow rate.

5. Acknowledgements

6. References

[1] Brouns, M. Verbanck, S and Lacor, C. accepted October 2005. Influence of glottic aperture on the tracheal flow, Journal of Biomechanics

[2] Corcoran, T. Chigier, N. 2000. Characterization of the Laryngeal Jet Using Phase Doppler Interferometry, Journal of Aerosol Science 13, 125-137.

[3] Gemci, T. Corcoran, T., Chigier, N., 2000. Dispersion and deposition of inhalation therapy sprays in the larynx and trachea using experimental and numerical methods. In Proceedings of the International Conference on Liquid Atomization and Spray Systems, Passadena

[4] Gosmann and Ioannides (1981): Aspects of computer simulation of liqued-fueled combustors. *AIAA* 81-0323.

[5] Hart D.P., 1996. Sparse array image correlation, Proc. 8th International Symposium on Appl. Of Laser Techniques to Fluid Mechanics, 8-11 July, Lisbon, Portugal

[6] Heenan, A. Matida, E. Pollard, A. Finlay, W., 2003. Experimental measurements and computational modeling of the flow field in a idealized human oropharynx. Experiments in Fluids 35, 70–84.

[7] Katz, I. Martonen, T., 1996. Flow patterns in three-dimensional laryngeal models. Journal of Aerosol Medicine 9, 501-511.

[8] Keane R.D., Adrian R.J., 1992. Theory of cross-correlation analysis of PIV images. Appl Sci Res 49:191-215

[9] Kleinstreuer, C. Zhang, Z., 2003. Laminar-to-turbulent fluid-particle flows in a human airway model. International Journal of Multiphase Flow 29, 271–289.

[10] Matida, E.A. Finlay, W.H. Lange, C.F. Grgic, B., 2004. Improved numerical simulation of aerosol deposition in an idealized mouth–throat. J. Aerosol Science 35, 1-19

[11] Martonen, T.B., Quan, L., Zhang, Z. and Musante, C.J., 2002, Flow simulation in the human upper respiratory track. Cell Biochemistry and Biophysis 37, 27-36

[12] Raffel, M., Willert, C., Kompenhans, J.,. Particle Image Velocimetry – a practical guide. Springer, Berlin Heidelberg New York, ISBN 3-540-63683-81998

[13] Renotte, C. Bouffioux, V. Wilquem, F., 2000. Numerical 3D analysis of oscillatory flow in the time-varying laryngeal channel. Journal of Biomechanics 33, 1637-1644.

[14] Yu G., Zhang Z., Lessmann R., 1998. Fluid flow and particle diffusion in the human upper respiratory system. Aerosol Science and Technolgy 28, 146-158

[15] Zhang, Z. Kleinstreuer, C. Kim, C., 2002. Micro-particle transport and deposition in a human oral airway model. Journal of Aerosol Science 33, 1635–1652